◆ Human Brain Mapping 31:1727–1740 (2010) ◆

Whole Brain-Based Analysis of Regional White Matter Tract Alterations in Rare Motor Neuron Diseases by Diffusion Tensor Imaging

Alexander Unrath, Hans-Peter Müller, Axel Riecker, Albert C. Ludolph, Anne-Dorte Sperfeld, and Jan Kassubek*

Department of Neurology, University of Ulm, Ulm, Germany

Abstract: Different motor neuron disorders (MNDs) are mainly defined by the clinical presentation based on the predominance of upper or lower motor neuron impairment and the course of the disease. Magnetic resonance imaging (MRI) mostly serves as a tool to exclude other pathologies, but novel approaches such as diffusion tensor imaging (DTI) have begun to add information on the underlying pathophysiological processes of these disorders in vivo. The present study was designed to investigate three different rare MNDs, i.e., primary lateral sclerosis (PLS, $N = 25$), hereditary spastic paraparesis (HSP, $N = 24$), and X-linked spinobulbar muscular atrophy (X-SBMA, $N = 20$), by use of whole-brain-based DTI analysis in comparison with matched controls. This analysis of white matter (WM) impairment revealed widespread and characteristic patterns of alterations within the motor system with a predominant deterioration of the corticospinal tract (CST) in HSP and PLS patients according to the clinical presentation and also in patients with X-SBMA to a lesser degree, but also WM changes in projections to the limbic system and within distinct areas of the corpus callosum (CC), the latter both for HSP and PLS. In summary, DTI was able to define a characteristic WM pathoanatomy in motor and extra-motor brain areas, such as the CC and the limbic projectional system, for different MNDs via whole brain-based FA assessment and quantitative fiber tracking. Future advanced MRI-based investigations might help to provide a fingerprint-identification of MNDs. *Hum Brain Mapp 31:1727–1740, 2010.*

Key words: diffusion tensor imaging; motor neuron diseases; PLS; HSP; X-SBMA

INTRODUCTION

The clinical spectrum of motor neuron diseases (MNDs) ranges from disorders that are limited to lower motor neurons (LMN) to those that exclusively affect upper motor neurons (UMN), such as hereditary spastic paraplegia (HSP) and primary lateral sclerosis (PLS). In the first instance, these neurodegenerative diseases can be distinguished by the more or less specific patterns of their clinical presentation and additional laboratory findings, as specified in clinical diagnostic criteria [Harding, 1993; La Spada et al., 1992; Pringle et al., 1992]. In this neuroimaging study, three rare MNDs with different motor neuron involvement were investigated with respect to their in vivo brain pathoanatomy, i.e., PLS, HSP, and the LMN disorder X-linked spinobulbar muscular atrophy (X-SBMA).

Pringle et al. proposed diagnostic criteria for PLS, including that the most common manifestations of PLS are

Additional Supporting Information may be found in the online version of this article.

*Correspondence to: Jan Kassubek, Department of Neurology, University of Ulm, Oberer Eselsberg 45, 89081 Ulm, Germany. E-mail: jan.kassubek@uni-ulm.de

Received for publication 28 May 2009; Revised 21 October 2009; Accepted 13 November 2009

DOI: 10.1002/hbm.20971

Published online 24 March 2010 in Wiley Online Library (wileyonlinelibrary.com).

spastic leg and pseudobulbar paresis that tend to follow a very slow, gradually progressive course and adult onset [Pringle et al., 1992]. Supportive laboratory tests merely help to exclude other diseases [Singer et al., 2007]. In some cases, focal atrophy of the precentral gyrus and thinning of the motor cortex on magnetic resonance imaging (MRI) [Butman and Floeter, 2007], and decreased glucose consumption in pericentral regions on positron emission tomography (PET) scan have been observed [Turner et al., 2007]. Magnetic resonance spectroscopy (^{1}H MRS) studies revealed reduced metabolite ratios in PLS patients compared to controls, suggesting dysfunction or loss of neurons in the motor cortex. Lastly, diffusion tensor imaging (DTI) has demonstrated decreased fractional anisotropy (FA) in the internal capsule, which implies damage to or dysfunction of these white matter (WM) structures [Ulug et al., 2004]. Recently, a study based on the FA analysis technique known as tract-based spatial statistics (TBSS) [Smith et al., 2006], which was performed in patients with amyotrophic lateral sclerosis (ALS) and PLS, showed widespread alterations of the FA in motor and extra-motor brain areas in both patient groups in comparison to healthy controls [Ciccarelli et al., 2009].

As a heterogeneous group of rare inherited neurodegenerative disorders of the upper motor neuron, HSP is characterized by a progressive spasticity of the lower limbs and gait or bladder disturbances with a variable occurrence of symptoms and age of onset [Fink, 2006]. The diagnosis is based upon clinical features, and phenotypic variability has led to a classification into pure (HSP) and complicated forms (cHSP in which spastic paraplegia is accompanied by major nonmotor findings out of a wide spectrum) [Fink et al., 1996; McDermott et al., 2000]. Besides the presumably nonspecific findings such as subcortical and periventricular WM lesions that are detected by conventional MRI, the most obvious finding in complicated subtypes of HSP is a thin corpus callosum (CC) [Shibasaki et al., 2000]. Further, an impressive pattern of gray and even more white matter deterioration was reported in patients with pure and complicated HSP by use of voxel-based morphometry (VBM) methods [Kassubek et al., 2007a], while recently, a case study described widespread WM effects in terms of ^{1}H MRS-based findings as well as reduced FA detected via DTI [Dreha-Kulaczewski et al., 2006]. Taken together, these findings indicate that the underlying pathological process in HSP affects large parts of the white matter of the CNS.

X-SBMA, also named Kennedy disease, is clinically characterized by an adult-onset slowly progressive MND with impairment of the lower motor neuron and a focus on the proximal muscular atrophy of the upper limb and bulbar muscles and additional symptoms due to partial androgen insensitivity [Sperfeld et al., 2002], but subtle involvement of other neurological systems has been shown to be part of the clinical spectrum [Buecking and Pfister, 2000]. Using advanced MRI techniques, ^{1}H MRS studies have shown significant alterations in the metabolite ratios in parts of the brainstem and motor regions of the brain as well as the involvement of cortical structures [Mader et al., 2002]. A recent voxel-based morphometry (VBM) study brought evidence for extensive WM atrophy particularly in frontal lobe areas as well as in the brainstem and cerebellum [Kassubek et al., 2007b].

Taken together, a common feature of the MNDs that are all clinically different from the most common adult-onset MND, i.e., ALS, seems to be the variable impairment of supratentorial brain areas, especially of WM structures. DTI has proven to be a valuable tool for analyzing WM alterations [Ciccarelli et al., 2008; Mukherjee et al., 2002; Salat et al., 2005; Snook et al., 2005], so the purpose of this study was to apply DTI to brain MRI data of patients with the above-named MNDs to analyze and quantify WM tract integrity by a whole brain-based approach and fiber tracking (FT), with the aim of producing a DTI-based definition of disease-associated patterns of microstructural WM alterations that might correlate with the clinical presentation.

METHODS

Subjects and Clinical Characterization

All patients underwent standardized clinical, neurological, and routine laboratory examinations. The patients of the different MND groups and the corresponding healthy controls were all right handed. All subjects gave written informed consent for the MRI protocol according to institutional guidelines which was approved by the Ethical Committee of the University of Ulm. Data on the subject groups are provided in Table I.

Twenty-five consecutive patients who met the diagnostic criteria for PLS proposed by Pringle et al. [1992] were included in the study. Further mandatory criteria for inclusion were negative tests for multiple sclerosis and for HIV and human T-lymphotropic virus Type 1 (HTLV-1), and routine MRI scans excluded, for example, Chiari malformation or cervical cord abnormalities. Disease duration in the PLS group was 6.6 ± 4.7 years, and age of onset of the motor disorder was 53.5 ± 8.6 years (all data are given as arithmetic mean ± standard deviation (SD)).

In the HSP group, all 24 patients fulfilled the published criteria for HSP, and possible differential diagnoses were excluded as suggested by Fink et al. [2006]. In 19 HSP cases, there was an autosomal-dominant inheritance pattern; in the other patients, the inheritance pattern could not be defined. Within the HSP group, there were six patients with spastin mutations; no further mutations were detected. The disease duration was 18.9 ± 13.3 years.

In all 20 X-SBMA patients, the diagnosis was genetically confirmed (mean number of CAG repeats 47.2 ± 2.4, range 42–50). Within the patient collective, there were three groups of three brothers each and one pair of first-line cousins. The mean age at manifestation of the disorder was 25.8 ± 12.1 years. The disease duration at the time of scanning was 22.3 ± 9.1 years. All patients showed typical

TABLE I. Characteristics of the subject groups

	PLS patients	PLS controls
Age (mean ±SD)	60.0 ± 9.0	57.0 ± 12.5
Gender (m/f)	8/17	8/17
	HSP patients	HSP controls
Age (mean ±SD)	50.0 ± 9.3	48.0 ± 13.7
Gender (m/f)	12/12	12/12
	X-SBMA patients	X-SBMA controls
Age (mean ±SD)	49.7 ± 8.2	49.7 ± 15.5
Gender (m/f)	20/0	20/0

PLS, HSP, and X-SBMA.

muscular spinobulbar tetraparesis, perioral and generalized fasciculations, and gynecomastia.

For each MND patient sample, a specific normal database was examined, consisting of 25 healthy controls for the PLS group, 24 controls for the HSP sample, and 20 healthy male subjects for comparison to the X-SBMA patients, respectively. The patient groups and the control groups did not differ in age so that all control groups were age- and gender-matched with their corresponding patient samples. None of the patients had a history of major psychiatric disorders or substance abuse, and neoplastic brain processes and vascular brain alterations were excluded by conventional MRI. The control samples had no history of neurological/psychiatric disease or other medical conditions.

MRI Acquisition

DTI scanning protocols were performed on a 1.5 Tesla Magnetom Symphony (Siemens Medical, Erlangen, Germany). The DTI study protocol consisted of 13 volumes (45 slices, 128 × 128 pixels, slice thickness 2.2 mm, pixel size 1.5 mm × 1.5 mm) representing 12 gradient directions and one scan with gradient 0 (b0). The echo time (TE) and repetition time (TR) were 93 ms and 8,000 ms, respectively; b was 800 s mm^{-2} and five scans were averaged online by the scanner software in image space. For the morphological background, a T1-weighted 3D magnetization-prepared rapid-acquisition gradient echo (MP-RAGE) was recorded for each patient and control subject (TR 9.7 ms, TE 3.93 ms, TI 880 ms, flip angle 15°, matrix size 256 × 256 pixels, FOV 250 mm, 192 slices, slice thickness 1.0 mm, voxel size 0.96 × 0.96 × 0.96 mm^3).

Postprocessing

The postprocessing and statistical analysis was performed by use of the DTI analysis software tensor imaging and fiber tracking (TIFT) [Mueller et al., 2007a]. First, the method proposed by Shen et al. [2004] was applied for the correction of eddy current-induced geometric distortions of the echo-planar imaging-based DTI datasets, which relies on collecting pairs of images with diffusion sensitizing gradients reversed, i.e., for the paired images that are distorted with eddy currents in opposite directions, a column-wise correction in the image domain along the phase-encoding direction was performed by searching for the maximum value of the crosscorrelation between two corresponding columns and applying opposite shifts and scales equal to half of the correction. Second, a spatial normalization routine including affine and nonaffine normalization steps for all individual DTI datasets was performed. For this normalization process, a study-specific fractional anisotropy (FA)-template and a study specific mean diffusivity (MD)-template were created for each group (PLS, HSP, and X-SBMA, respectively). This process was iterative, i.e., in the first step a scanner- and sequence-specific b0-template of this study based on the Montreal neurological institute (MNI) stereotactic standard space [Brett et al., 2002] was created by arithmetically averaging the b0-volumes of all subjects after affine transformation according to manually set landmarks. In the second step, following the basic ideas of Ashburner and Friston [1999], a nonaffine MNI normalization of the DTI datasets was performed by minimizing the mismatch between regional intensities of the b0-volume to be fitted and of the template according to the squared differences (χ^2). The resulting normalization matrices were then applied to the remaining volumes of the DTI dataset (b1–b12 images). After this normalization procedure, all individual DTI datasets were used for the calculation of the second-rank diffusion tensor $\vec{D}$, the Eigenvalues (λ_1, λ_2, λ_3), the Eigenvectors ($\vec{v}_1, \vec{v}_2, \vec{v}_3$), and the FA and the MD for quantification of the diffusion anisotropy, according to standard methods [Basser and Jones, 2002; Le Bihan, 2001].

To obtain the study-specific templates necessary for the nonaffine normalization process, FA-templates and MD-templates were defined for each group separately by averaging all individually derived FA-maps and MD-maps, respectively, of one group of patients and controls (e.g., PLS patients and PLS healthy controls). After having created the FA-template and the MD-template, a nonaffine normalization was applied to the FA-template as suggested by Smith et al. [2006]. The nonaffine normalization process to the FA-template and the MD-template, respectively, follows the basic ideas of Ashburner and Friston [1999]. The nonaffine registration to an FA-template/MD-template has the advantage that it provides more contrast in comparison to b0-images [Smith et al., 2006]. The parameters of these normalization steps have to be stored so that they can be considered during the fiber tracking process (see below).

For smoothing, the fact that the filter size influences the results of DTI data analysis has to be taken into consideration [Jones et al., 2005]. The matched filter theorem states that the width of the filter used to process the data should be tailored to the size of the difference one expects to see [Rosenfeld and Kak, 1982]. Under the assumption that the

motor system in the brain might be affected in the three motor neuron disorders, we focused the analysis on its WM components, i.e., the CST that are particularly prominent in the posterior limb of the internal capsule (PLIC). On the basis of anatomical observations in human brain atlases [Mai et al., 1997] that the extent of the PLIC is in the order of 10 mm, we used a 10 mm (FWHM) Gaussian filter for smoothing within the whole brain-based statistical analysis to achieve a good balance between sensitivity and specificity.

Whole Brain-Based Statistical Analyses

For the statistical comparison of the respective patient groups and their corresponding healthy subject groups, Student's *t*-test was performed voxelwise, i.e., the FA values of the patients' FA maps were compared with the FA values of the healthy volunteers' FA maps for each voxel separately. Prior to calculation, the FA maps were masked by a WM mask derived from a thresholding procedure by which FA values below 0.2 were not considered for calculation (cortical gray matter shows FA values up to 0.2) [Kunimatsu et al., 2004]. Furthermore, the *t*-test was only performed if at least 60% of the subjects per group had an FA value above the threshold of 0.2 in the respective voxel. The statistical results were corrected for multiple comparisons using the false-discovery-rate (FDR) algorithm at $P < 0.05$ [Genovese et al., 2002]. Further reduction of the alpha error was performed by a spatial correlation algorithm that eliminated isolated voxels or small isolated groups of voxels (cluster threshold size, 64 voxels). In addition to this statistical approach, a between-group comparison of the FA maps of the three patient groups was performed to show specifically altered WM architecture according to the clinically different appearance of these MNDs.

The results of the voxel-wise comparison of the FA maps (Figs. 1–3) were tested for their correlation with motor disability. Therefore, in each cluster the mean FA value for each patient was tested for its correlation with the revised functional rating scale for ALS patients [ALS-FRS-R; Cedarbaum et al., 1999] for all patients. The resulting correlation was then tested for significance [Press et al., 1992].

Tractography

To apply fiber tracking (FT) algorithms, separate data processing steps were performed. According to the methods described previously [Mueller et al., 2007b, 2009], averaged DTI data sets were generated for the three groups PLS, HSP, and X-SBMA, i.e., an averaged DTI dataset from the patients' data, an averaged DTI dataset for the controls, and an averaged DTI dataset for the corresponding patients and controls together. This averaging requires careful treatment of the orientational information, which is preserved during the normalization process according to techniques described by Alexander et al., 2001 [for details see Mueller et al., 2009]. Tractography was performed in each group separately in comparison with the corresponding controls by application of a fiber tracking algorithm (streamline tracking technique). The group-averaged DTI datasets for all subjects in each group were the basis for the consecutive FT, which was performed using manually defined seed points adjacent to the local maxima detected by the whole brain-based FA analysis within the CC and the PLIC. The locations of the seed points were identified by use of the color-coded averaged FA maps. Here, the whole body of the CC was defined as all red-coded voxels (*x*-directional) within the mid-sagittal plane, and the PLIC was defined as all blue-coded voxels (*z*-directional) within the axial plane, depicting both the largest extent of the thalamus and the most caudal parts of the splenium. After identification of the seeds, tractography was performed, and the voxels of the delineated fibers were defined as a group-specific mask. In the same way, for the between-group comparison of the MND groups, the group-specific DTI datasets were processed thoroughly as a prerequisite for the application of FT algorithms.

Tractwise Fractional Anisotropy Statistics

To quantify the tractography results, the technique of tractwise fractional anisotropy statistics (TFAS) [Mueller et al., 2007b] was applied. By this approach, the fiber tracts that were created on the averaged DTI dataset of all subjects of each group were used for the selection of the voxels that contribute to a comparison between (i) the patients' and the controls' FA maps calculated from each averaged DTI dataset and (ii) the patients' FA maps for the three different MNDs. All resulting voxels showing an FA value above 0.2 were considered for statistical analysis by Student's *t*-test. To display the results on a morphological background, the 3D T1 weighted datasets were normalized to MNI-space and arithmetically averaged; this normalization procedure was performed in analogy to the DTI datasets by use of a study-specific template [Mueller et al., 2007b].

RESULTS

Whole Brain-Based Statistical Analyses

In the whole brain-based comparison of the FA values of the three samples of MND patients with their corresponding controls at group level, multiple clusters of regional FA reductions were observed at $P < 0.05$ (corrected for multiple comparisons, FDR). Tables II–IV summarize the results of the statistical analysis, i.e., all areas yielding significant FA reductions, including the size and the coordinates of the voxels of highest significance in MNI standard space. By application of the

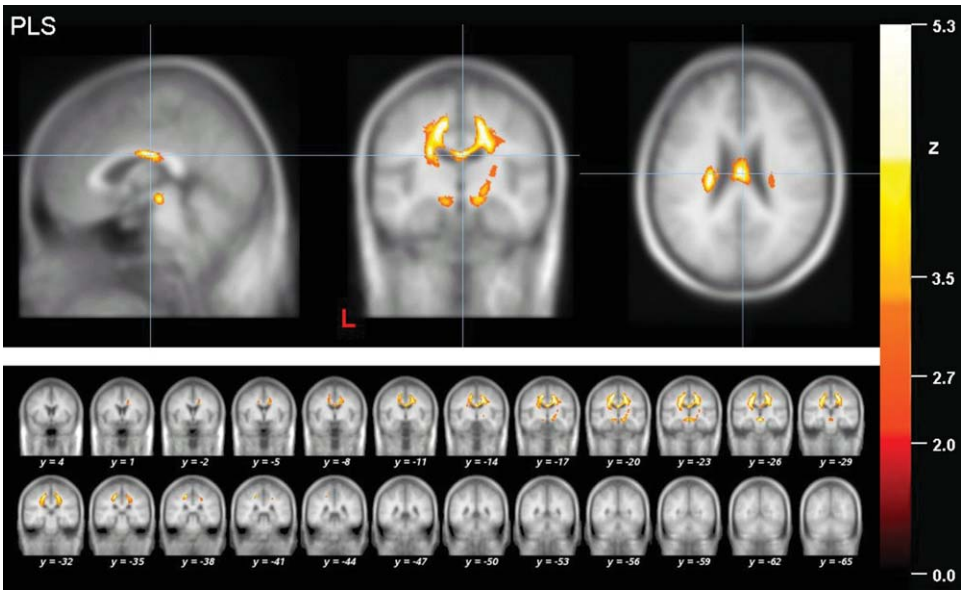

Figure 1.

Results of the whole brain-based analysis of the PLS patients. Local maximum of decreased FA values (thresholded at $P < 0.05$, corrected for multiple comparisons) in projections to the midbody of the corpus callosum (CC) in PLS patients in a sagittal, coronar and axial view (upper panel). The coronar multi-slice view (lower panel) exhibits widespread clusters of reduced FA values within subcortical WM areas of mainly the motor system including the CST and the CC as well as the projectional fiber system of the upper brain stem and the frontal lobe. The significance level (Z-score) is indicated by color temperature according to the scale (L = left).

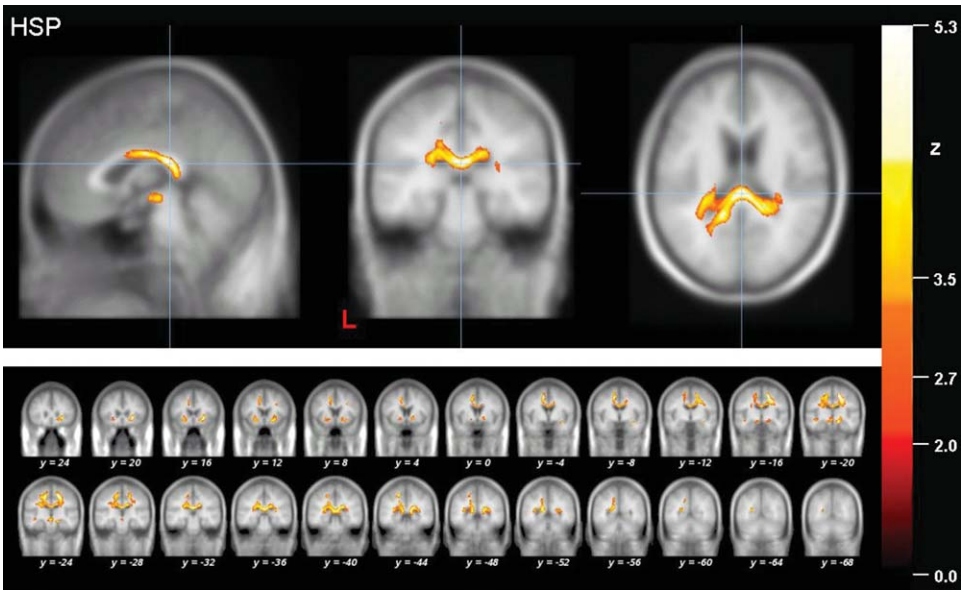

Figure 2.

Results of the whole brain-based FA analysis of the HSP patients. Local maximum of decreased FA values (thresholded at $P < 0.05$, corrected for multiple comparisons) in projection to the dorsal part of the CC in patients with HSP (upper panel). The multi-slice view shows significantly reduced FA values within subcortical WM areas of the motor and limbic system (lower panel).

TABLE II. Results of the DTI analysis of the PLS group (patients versus controls)

Cluster	MNI coordinates of maximum (mm)			Hemisphere (R = right; L = left)	Level of significance Z-score	Cluster size (number of voxels) n	Anatomical localization (white matter)
	x	y	z				
Motor system							
1	2	−20	25	R + L	6.3	11,898	CST, CC
2	−20	−25	40	L	6.5	10,182	CST, Corona radiata
3	−1	−27	−9	L	5.4	2,278	brain stem
4	26	−24	13	R	4.7	229	CST, PLIC

Results of the DTI analysis of the PLS group in comparison to the corresponding healthy subjects: areas of significant FA reduction, thresholded at $P < 0.05$ (FDR corrected). Levels of significance are given as mean Z-scores. Only the main contributing areas are listed while more anatomical structures are included in the cluster. MNI, Montreal Neurological Institute brain atlas; FDR, false discovery rate; CC, corpus callosum; CST, corticospinal tract; PLIC, posterior limb of the internal capsule.

statistical analysis provided by TIFT at a minimum cluster size of 64 voxels, four clusters were delineated in the PLS group within the subcortical white matter (Table II), while nine clusters were depicted in the HSP group (Table III), and twelve clusters were found in the X-SBMA group (Table IV).

In the PLS group, widespread alterations were observed in the supratentorial WM, in particular in projections to fiber tracts of the motor system including the corticospinal tracts (CST) of both hemispheres, and midbody parts of the corpus callosum and the brain stem (Fig. 1). Within the findings for the supratentorial WM, two large and almost symmetrical clusters were observed in widespread subcortical parts of the motor system. Notably, the result in the right hemisphere showed one connected cluster reaching from the corona radiata to the WM adjacent to the precentral gyrus and premotor cortical areas and extending to the midbody of the CC. The left-hemispherical cluster consisted of one large regional FA alteration that was located in projections to the PLIC, the corona radiata and the subcortical WM adjacent to the precentral gyrus and premotor cortical areas. Further significant WM changes were localized within ventral parts of the brain stem and in projections to the PLIC in the right hemisphere.

Whole brain-based statistical analysis of the HSP group data showed nine regional FA reductions (Fig. 2). There was a clear preponderance (10-fold higher voxel-count) of the three regions within the motor system in comparison to non-motor brain areas. In detail, one large contiguous FA reduction (39,667 voxels, overall) comprised large parts of the subcortical motor areas of the right hemisphere including the CST, reaching across the CC over to the left hemisphere, while the second cluster was depicted in the projection to the capsula extrema. One further cluster of significant FA reduction was localized within medial parts of the mesencephalon of the brain stem. The remaining six smaller regional WM changes that were localized in non-motor areas can be subsumed as parts of the limbic system and its projectional fiber system, namely one cluster was localized within the corpus amygdaloideum and two clusters were found adjacent to the precuneus and the parahippocampal cortex within the WM of the medial temporal gyrus. Within the right hemisphere, one cluster was adjacent to the cingulate gyrus and one cluster projected to the fasciculus uncinatus. Finally, one area within the WM of the middle/inferior frontal gyrus was found to have a significantly reduced in FA.

A distributed WM lesion pattern was observed in the X-SBMA group. The relationship between motor and nonmotor areas merely showed a 1.7-fold higher voxel-count, but, remarkably in this disorder with clinically prominent LMN impairment, two large and nearly symmetrically located clusters showed up in the projection to the CST of both hemispheres, involving 4,574 voxels on the right and 3,551 voxels on the left. Two additional clusters were located adjacent to the left-sided precentral gyrus and in the projection to the external pallidum (Fig. 3), indicating the involvement of the central motor system despite clinical LMN involvement. Further WM alterations were located within the limbic system or its projectional network, i.e., bilaterally adjacent to the precuneus, the temporal lobe, and inferior frontal lobe of the left hemisphere, and adjacent to the posterior cingulum. One additional area of significant FA reduction was located in the projection to the centrum semiovale of the left hemisphere.

The between-group comparison of the investigated MNDs revealed widespread differences within the motor system and the CC and, to a lesser degree, within limbic projectional fibers for X-SBMA compared to HSP as well as for X-SBMA versus PLS. Direct comparison of the HSP and the PLS group also showed distinct WM alterations for each group, shown as a decrease (corresponding to a higher FA value for the significant voxels in the HSP group compared to the PLS group) or an increase (FA(HSP) < FA(PLS)).

The results of the MD analysis are presented in terms of a "cojoint"-analysis, where the FA and the MD results (thresholded at $P < 0.05$, FDR corrected) are displayed

TABLE III. Results of the DTI analysis of the HSP group (patients versus controls)

Cluster	MNI coordinates of maximum (mm) x	y	z	Hemisphere (R = right; L = left)	Level of significance Z-score	Cluster size (number of voxels) n	Anatomical localization (white matter)
Motor system							
1	20	−25	49	R + L	5.6	39,667	CST, CC
2	26	18	−5	R	5.7	3,568	Capsula extrema
3	−3	−25	−8	L	5.1	1,252	Brain stem (mesencephalon)
Limbic system and projectional fibers							
4	−24	12	−11	L	5.0	1,628	Corpus amygdaloideum
5	17	−23	−15	R	5.4	1,083	Adjacent to the cingulate gyrus
6	−20	−45	54	L	5.3	739	Adjacent to the precuneus
7	−44	−21	−8	L	4.7	408	Parahippocampal lobe
8	34	−6	−16	R	5.4	306	Fasciculus uncinatus
9	32	11	30	R	5.3	157	Adjacent to the middle/inferior frontal gyrus

Results of the DTI analysis of the HSP group in comparison to the controls: areas of significant FA reduction, thresholded at $P < 0.05$ (FDR corrected). For levels of significance, anatomical localizations and abbreviations, cf. Table 2.

together (Fig. 4). A total of five areas of significantly increased MD values were observed in the PLS group, while in the HSP group only three clusters could be delineated, whereas there was no statistically significant change in MD in the X-SBMA group in the whole brain-based analysis. Remarkably, the largest areas of significantly increased MD were observed in juxtacortical WM regions adjacent to or overlapping with the regions of significantly decreased FA. In detail, one large cluster was found in the PLS group within the right hemisphere, two clusters were depicted in the projection to the left-hemispheric subcortical areas of the motor system and one cluster was localized in lateral parts of the left-hemispheric CC. One additional regional MD increase was located within the inferior parietal lobe adjacent to the precuneus. In the HSP group analysis, all clusters were observed within WM areas corresponding to the CST or further parts of the motor system with a predominance in the right hemisphere. No reductions in MD values were observed in any of the group analyses.

There were no statistically significant correlations between WM alterations and disease duration or the extent of motor disability (ALS-FRS-R) in any of the three MNDs.

TABLE IV. Results of the DTI analysis of the X-SBMA group (patients versus controls)

Cluster	MNI coordinates of maximum (mm) x	y	z	Hemisphere (R = right; L = left)	Level of significance Z-score	Cluster size (number of voxels) n	Anatomical localization (white matter)
Motor system							
1	27	−18	35	R	4.8	4,574	CST
2	−27	−18	27	L	5.1	3,551	CST
3	−10	−31	53	L	4.6	554	Adjacent to the precentral gyrus
4	25	−13	−2	R	4.2	453	External pallidum
Limbic system and projectional fibers							
5	−21	−53	52	L	4.6	2,249	Adjacent to the precuneus
6	−21	−78	27	L	5.0	1,312	Adjacent to the precuneus
7	−47	−21	−11	L	5.3	574	Middle temporal lobe
8	−37	38	−2	L	4.5	391	inferior frontal lobe
9	26	−58	39	R	4.2	360	Adjacent to the precuneus
10	−41	−65	5	L	5.1	274	Middle temporal lobe
11	−14	−55	24	L	4.4	225	Adjacent to the posterior cingulum
Additional clusters: projectional fibers							
12	−33	−45	28	L	4.6	1,279	Centrum semiovale

Results of the DTI analysis of the X-SBMA group in comparison to the controls: areas of significant FA reduction, thresholded at $P < 0.05$ (FDR corrected). For levels of significance, anatomical localizations and abbreviations, cf. Table 2.

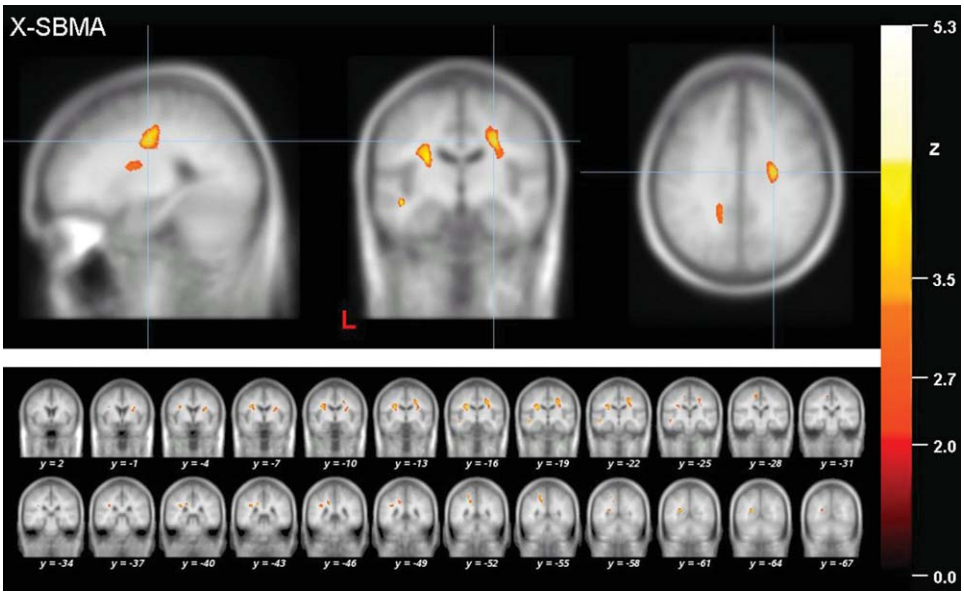

Figure 3.

Results of the whole brain-based FA analysis of the X-SBMA patients. Local maximum of decreased FA values (thresholded at $P < 0.05$, corrected for multiple comparisons) in projections to the CST in patients with X-SBMA (upper panel). The multi-slice view shows significantly reduced FA values within subcortical WM areas of the motor and limbic system (lower panel).

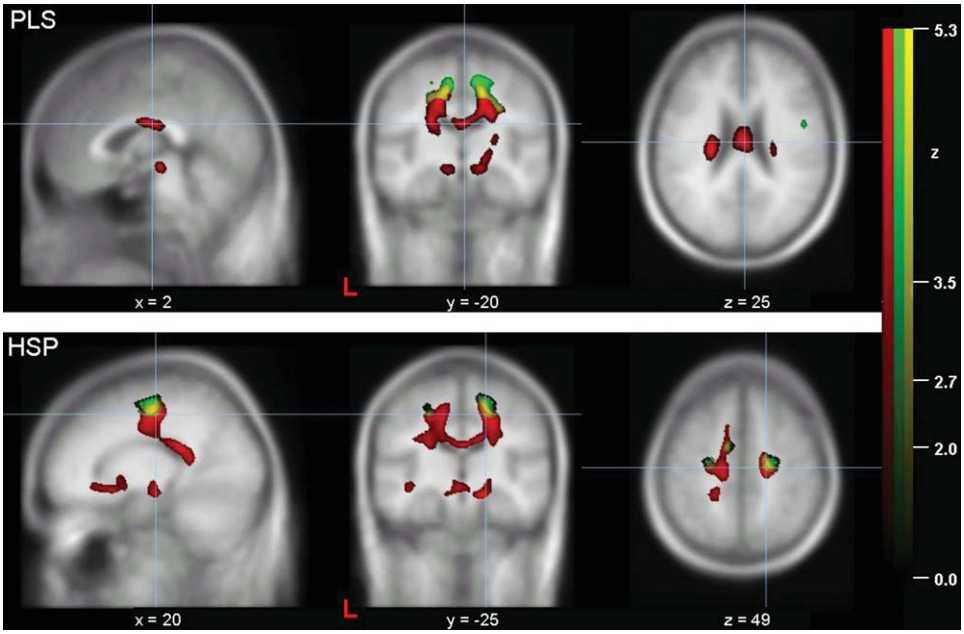

Figure 4.

Results of the cojoint whole brain-based analysis of the PLS patients and the HSP patients: Cojoint display of decreased FA values (red) and increased MD values (green) (each thresholded at $P < 0.05$, corrected for multiple comparisons) in PLS patients (upper row) and in HSP patients (lower row). The overlap between significantly decreased FA and significantly increased MD is color-coded in yellow. The significance level (*Z*-score) is indicated by color intensity according to the scale (red—significant FA decrease, green—significant MD increase, yellow—overlap) (L = left).

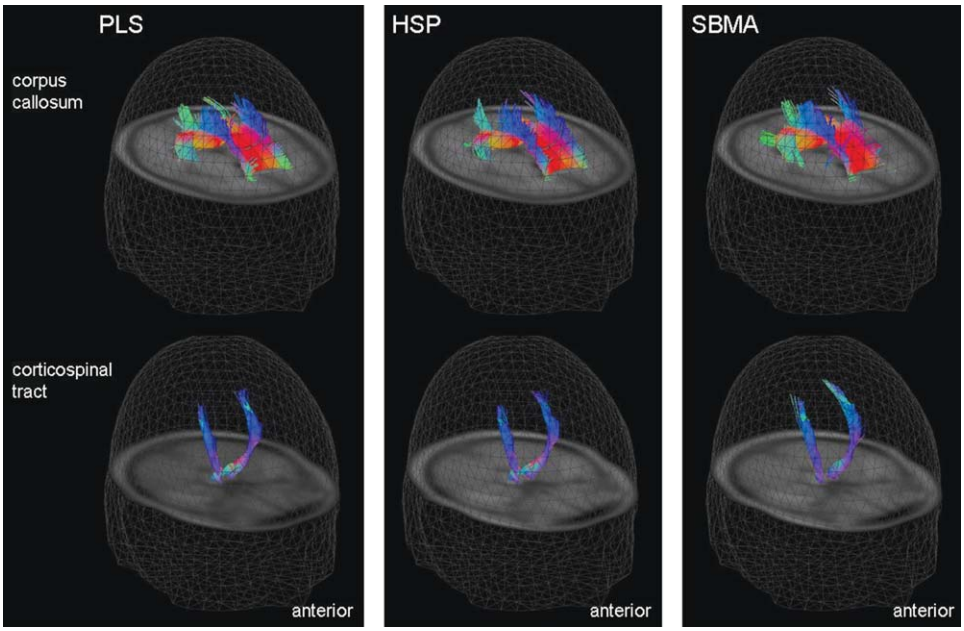

Figure 5.

Results of the fiber tracking (FT) analysis of the PLS patient group (left column), the HSP patient group (center column), and the X-SBMA patient group (right column). The 3D view of the comparison of tractography results with seed points within the areas of significantly reduced FA values in the CC (upper row) and in the posterior limb of the internal capsule (PLIC) of both hemispheres (lower row). According to color-coding conventions, red means right-left, green means anterior-posterior and blue means cranio-caudal directionality. FT was performed on averaged DTI datasets that were created by arithmetically averaging all MNI-normalized single subject DTI datasets of one group (e.g., all PLS patients and the corresponding controls).

Tractwise Fractional Anisotropy Statistics

The quantitative TFAS analysis revealed statistically significant differences in fiber FA crossing the CC and within the CST between patients and controls in the PLS and the HSP group analyses (Fig. 5). In X-SBMA, the TFAS analysis of the CST was also significant while the evaluation of the CC and its projectional fiber system was not significant (Table V). The latter result is in accordance with the whole brain-based statistical analysis, in which significant alterations in the CST were observed while no clusters of reduced FA were depicted in projections to the CC. Direct comparison of the three MNDs by application of TFAS confirmed the findings of the whole brain-based approach and showed significant differences in tract integrity within the CC for X-SBMA versus HSP and versus PLS, for HSP versus PLS and also within the CST for X-SBMA versus PLS and for HSP versus PLS (Fig. 6, Table VI). The results of the TFAS analyses are presented in Table V (each MND compared to the respective healthy controls group) and Table VII (between group comparison of the MNDs).

DISCUSSION

By use of whole brain-based DTI [Mueller et al., 2007a], characteristic patterns of regional WM alterations in the brain in terms of significantly altered FA values were observed in the three different groups of MNDs, namely in patients with PLS, HSP, and X-SBMA. In PLS and HSP, widespread alterations were observed within the motor system. In addition, as expected for patients with HSP on the basis of recent findings obtained using VBM [Kassubek et al., 2007a] but not yet reported for patients with

TABLE V. Results of the TFAS (tractwise fractional anisotropy statistics) analysis

	FA patients	FA controls	No. voxels	*t*-test
PLS				
CC	0.29 ± 0.10	0.36 ± 0.11	10,841	<0.001
CST	0.38 ± 0.11	0.41 ± 0.12	3,841	<0.001
HSP				
CC	0.31 ± 0.08	0.37 ± 0.11	18,451	<0.001
CST	0.41 ± 0.12	0.43 ± 0.11	3,958	<0.001
X-SBMA				
CC	0.35 ± 0.12	0.35 ± 0.12	21,497	0.34
CST	0.42 ± 0.12	0.44 ± 0.13	4,257	<0.001

Tractwise fractional anisotropy (TFAS) results for the PLS-group, the HSP-group, and for the X-SBMA-group. Data are presented as mean values ± SD. A *t*-test was performed for the comparison between mean FA values of patients and controls.

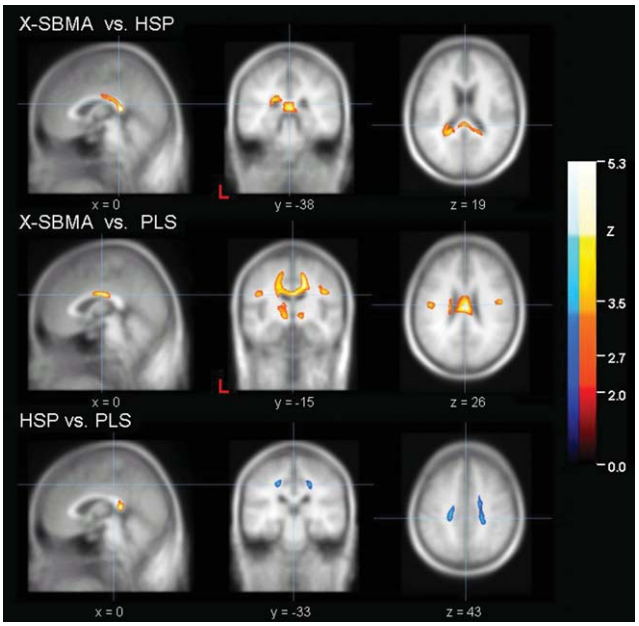

Figure 6.

Upper row: significant FA decrease between X-SBMA patients and HSP patients. Display focus is the splenium of the corpus callosum (MNI $(x,y,z) = (0, -38, 19)$). Central row: significant FA decrease between X-SBMA patients and PLS patients. Display focus is the midbody of the corpus callosum (MNI $(x,y,z) = (0, -15, 26)$). Lower row: significant differences between HSP patients and PLS patients, where FA reduction (FA(HSP) > FA(PLS)) is encoded red and FA increase (FA(HSP) < FA(PLS)) is encoded blue. The display focus was chosen to display FA differences within the motor system (MNI $(x,y,z) = (0, -33, 43)$). All data are thresholded at $P < 0.05$ and FDR corrected, including a cluster threshold of 64 voxels.

PLS except in one study with a sample size of six [Ciccarelli et al., 2009], WM alterations were observed in projections to dorsal (HSP) and midbody (PLS) parts of the corpus callosum. In patients with X-SBMA, the pattern of significant clusters of reduced FA within the WM showed significant alterations in the CST bihemispherically besides disseminated clusters within the limbic system and its projectional fiber system. Increased MD values were observed in the juxtacortical WM corresponding to the motor system of both hemispheres in close proximity and partly overlapping with the findings of the FA analyses in the PLS and HSP groups, while no altered MD was found in the X-SBMA group in the whole brain-based approach. In a nutshell, MD does not seem to be an adequate parameter for detecting the full extent of WM disintegrities in selected neurodegenerative diseases, but may complement the information provided by FA. To further address the findings of altered CC and CST integrity, quantitative FT algorithms were applied to the DTI data, demonstrating significantly altered tract integrity within the delineated fiber pathways of the motor system (CST) and callosal association fibers (CC). To identify the different and specific lesion patterns of the three presented MND subtypes, direct comparison based on whole brain-based and tractwise FA statistics of these diseases were used to reveal characteristically different vulnerability patterns throughout large parts of the motor and limbic projectional fiber system, with special focus on the CST and the CC, which both reflect hallmarks of the presented analyses.

Impact of DTI Analyses in Lower Motor Neuron Diseases

Basically, different MNDs beyond ALS show different clinical patterns with respect to the degree of affectation of the UMN or LMN. In X-SBMA, the clinically obvious vulnerability pattern is limited to the LMN, but it is increasingly recognized that this disease also affects the CNS to a certain extent, e.g., frontal brain areas. Conventional MRI investigations provide little to support these clinical considerations. Advanced MRI methods such as ^{1}H-MRS [Karitzky et al., 1999] and optimized VBM [Kassubek et al., 2007b] have brought evidence for widespread WM deterioration in X-SBMA patients. Thus, the results of the present study do not only confirm previous findings of WM disruption to a large extent, but also demonstrate the involvement of limbic structures. This finding of limbic involvement is notable since several studies provided evidence that higher-order cognitive functions are impaired in association with amyotrophic lateral sclerosis, especially with bulbar-onset disease [Abrahams et al., 1997; Schreiber et al., 2005]. For X-SBMA patients, it has been shown that the clinical phenotype often includes cognitive deficits as well as behavioral abnormalities [Guidetti et al., 1996], and a neuropsychological study has demonstrated that fronto-temporal cognitive functions are impaired in SMBA, although at a subclinical level [Soukup et al., 2009]. Within the concept of frontal deficits as part of the pathological spectrum of MNDs, the limbic WM structures, with their close connection to frontal areas, were found to be involved in X-SBMA (and, to a lesser degree, in HSP). Furthermore, significantly reduced FA in X-SBMA was also observed in projections to the CST of both hemispheres which probably reflects the anatomical expression of a possible axonal degeneration of the UMN in the course of MND [Karlsborg et al., 2004]. The underlying pathophysiology of degeneration in MNDs has not yet been clarified, and there is an ongoing debate on antero- or retrograde degenerative processes and the influence of nonneuronal cells on the loss of motor neurons [Clement et al., 2003]. As DTI methods fail to differentiate between antero- and retrograde degeneration, this question could not be addressed by the technical approach of the present study.

TABLE VI. Results of the whole brain-based between group FA analyses

Cluster	MNI coordinates of maximum (mm) x	y	z	Hemisphere (R = right; L = left)	Level of significance Z-score	Cluster size (number of voxels) n	Anatomical localization (white matter)
A. X-SBMA versus HSP							
FA decrease							
1	0	−43	12	−/R	5.4	7,808	CC
2	−25	−10	−8	L	5.3	1,638	Adjacent to the parahippocampal gyrus
3	17	−25	53	R	5.3	1,610	Adjacent to the precentral gyrus
4	48	−16	31	R	4.7	486	Adjacent to the precentral gyrus
5	25	17	−1	R	5.3	424	External capsule
B. X-SBMA versus PLS							
FA decrease							
1	16	−21	39	R	5.4	19,941	Adjacent to the cingulate gyrus
2	−12	−19	−4	L	5.1	3,291	Brain stem (mesencephalon)
3	18	42	−3	R	5.4	2,246	Adjacent to the anterior cingulum
4	49	−13	29	R	5.3	1,384	Adjacent to the precentral gyrus
5	13	−22	−6	R	5.3	1246	Brain stem (mesencephalon)
6	−47	−17	27	L	4.6	633	CST
7	−5	26	6	L	5.4	287	CC
C. HSP versus PLS							
FA decrease							
2	−2	−43	12	L	5.7	3357	CC
3	−20	1	−3	L	5.3	2681	Putamen
6	22	5	1	R	4.1	439	Putamen
FA increase							
1	23	4	30	R	4.7	4,161	Prefrontal centrum semiovale
4	−22	−32	44	L	4.5	1,395	Adjacent to the postcentral gyrus
5	−20	10	32	L	4.0	628	Adjacent to the cingulate gyrus
7	−12	−21	54	L	5.2	224	Adjacent to the precentral gyrus

Results of the statistical between group analyses of the DTI datasets of the three investigated MNDs (part A: X-SBMA versus HSP; part B: X-SBMA versus PLS; part C: HSP versus PLS). MNI coordinates display the maximum within the areas of significant FA reduction, thresholded at $P < 0.05$ (FDR corrected). For levels of significance, anatomical localizations and abbreviations, cf. Table 2.

DTI Analyses in Upper Motor Neuron Diseases

In contrast to X-SBMA, both HSP and PLS are characterized by a clinical impairment almost exclusively in the UMN. In line with previous observations [Kassubek et al., 2006, 2007a; McDermott et al., 2000], the present DTI-based study demonstrated an altered WM architecture in projections to the above-named dorsal parts of the CC, along with large significant FA reductions in frontal WM areas as well as in parts of the limbic system and its projectional fibers. These findings may lead to a new perspective on the underlying neurodegenerative process with respect to its pathoanatomy in the central nervous system. Whilst the pathophysiological process of the assumed neurodegeneration in HSP remains speculative [Alber et al., 2005; Sperfeld et al., 2004], microstructural alterations depicted by DTI might, based on a certain likelihood, precede the development of macroscopically detectable atrophy [Mukherjee and McKinstry, 2006]. Here, DTI demonstrates its potential to reveal much more widespread damage to WM areas, e.g., the CST and premotor areas. However, the fact that there was no correlation between motor disability and the degree of WM abnormalities may serve as an argument for a developmental variant of the CC in HSP or at least for a reduced specificity; this is also indicated by previous findings of altered CC anatomy in preterm birth and the vulnerability of the CC in perinatal WM injury [Back et al., 2001].

Importantly, significantly decreased FA was also found in projections to the CC in the PLS group, located ventrally in the CC midbody. These findings in the interhemispheric CC suggest a widening of the pathoanatomical pattern of PLS, since mainly ROI-based investigations at different levels of the CST by DTI have been reported to date [Chan et al., 2003; Ulug et al., 2004]. Our findings are consistent with the results of a recent study by Ciccarelli et al. [2009] who reported significantly altered FA values in motor and nonmotor brain areas. Here, the authors investigated a sample of six patients with PLS by using a technique based on the quantification of FA values within selected fiber tracts, known as TBSS [Smith et al., 2006], and found reduced FA in WM structures adjacent to the precentral gyrus and in projections to the body of the CC. In accordance with the clinical presentation, the present

TABLE VII. Between group analyses by TFAS

	HSP patients	X-SBMA patients	No. voxels	*t*-test
X-SBMA versus HSP				
CC	0.33 ± 0.10	0.38 ± 0.13	16,825	<0.001
CST	0.42 ± 0.14	0.43 ± 0.14	4,413	0.095
	HSP patients	PLS patients	No. voxels	*t*-test
X-SBMA versus PLS				
CC	0.32 ± 0.11	0.39 ± 0.14	12,355	<0.001
CST	0.39 ± 0.13	0.43 ± 0.15	4,388	<0.001
	PLS patients	X-SBMA patients	No. voxels	*t*-test
HSP versus PLS				
CC	0.36 ± 0.10	0.34 ± 0.11	9,951	<0.001
CST	0.43 ± 0.14	0.40 ± 0.12	4,277	<0.001

Tractwise fractional anisotropy (TFAS) results for between group analyses of the three investigated MNDs. Data are presented as mean values ± SD. A *t*-test was performed for the comparison between mean FA values of X-SBMA and HSP, X-SBMA and PLS and HSP and PLS, respectively.

whole brain-based study demonstrated extensive deterioration of motor areas with large regional FA reductions within the CST, similar to findings reported for ALS [Sach et al., 2004; Sage et al., 2007]. In the same way, premotor areas were found to be affected (in a "horseshoe-like" pattern where the convexity of this semilunar cluster is located within the CC and both ends point to the cortical representation areas), which correlates well with subcortical areas of projectional fibers of the lower limbs and therefore appears consistent with the clinical preponderance of spasticity in the legs. One possible explanation of altered CC anatomy in both PLS and HSP patients with respect to the clinical presentation is that the degeneration of the pyramidal tracts as found in MNDs with a UMN preponderance may be accompanied by degeneration of callosal association fibers. However, these findings give clear evidence for WM impairment beyond CST degeneration in PLS patients, and further investigations should also address the CC as a relevant part of the PLS-associated pathoanatomy.

Tractography and Tractwise Fractional Anisotropy Statistics

The quantitative FT analysis by application of TFAS allowed selective analysis of the anatomico-functional tract systems associated with the respective disease. For the CST, quantitative FT analysis demonstrated highly significant alterations in all three motor neuron disorders, indicative of its potential use as a biomarker at the group level. In particular, for X-SBMA, which is a disorder with clinically prominent LMN impairment, this observation of alterations in UMN tract integrity is relevant to its understanding as a multisystem disorder. Concerning the abovementioned supposed degeneration of callosal association fibers in UMN-dominated disorders, the finding of unaltered CC anatomy in X-SBMA by TFAS supports this hypothesis. Therefore, a quantitative evaluation of tractographies may widen the understanding of either of the pathologies examined if combined with the results of the whole brain-based analysis in terms of a complementary interpretation.

General Considerations

In patients with neurodegenerative diseases, WM atrophy often exists to a certain degree, as shown in studies using voxel-based morphometric approaches [Kassubek et al., 2007a,b]. The extent of atrophy might influence the results of the FA analysis, as recently shown in a study by Vernooij et al. [2008] concerning age-related alterations in WM integrity in a large cohort of healthy controls aged ≥60 years. In that study, the authors also reported that voxel-based statistical analyses in particular are prone to misinterpretation of macroscopic brain involution processes and that altered microstructural WM integrity might be caused by different pathophysiological developments. Although the influence of atrophy on the results cannot be completely eliminated, the methodological concept of the postprocessing steps, particularly the normalization processing, took into account the potential confounding effect of changes in WM volume on the results to diminish the influence of atrophy. In detail, a sequence- and scanner-specific template was generated including all subjects of a certain group, i.e., both the patient group and the healthy controls [Good et al., 2002], which was subsequently used for the normalization of the individual subjects. Thus, potential atrophic alterations in the patients' brains are considered in depth within the normalization procedure compared to a normalization procedure using a nonspecific template.

CONCLUSIONS

In summary, the present whole brain-based analysis showed characteristic lesion patterns correlated with the involvement of certain distinct brain areas within the specific pathological processes of the three investigated rare MND types. The CC seems to be a key structure experiencing microstructural disruption of the WM tract in MNDs with the clinical predominance of UMN impairment, although even here, the pattern of CC alterations in HSP and PLS was characteristically different. Consequently, DTI-based methods may be an additional tool for defining the pathoanatomy of MND subtypes by microstructural in vivo fingerprint characteristics.

REFERENCES

Abrahams S, Goldstein LH, Al-Chalabi A, Pickering A, Morris RG, Passingham RE, Brooks DJ, Leigh PN (1997): Relation between cognitive dysfunction and pseudobulbar palsy in amyotrophic lateral sclerosis. J Neurol Neurosurg Psychiatry 62:464–472.

Alber B, Pernauer M, Schwan A, Rothmund G, Hoffmann KT, Brummer D, Sperfeld AD, Uttner I, Binder H, Epplen JT, Dullinger J, Ludolph AC, Meyer T (2005): Spastin related hereditary spastic paraplegia with dysplastic corpus callosum. J Neurol Sci 236:9–12.

Alexander DC, Pierpaoli C, Basser PJ, Gee JC (2001): Spatial transformations of diffusion tensor magnetic resonance images. IEEE Trans Med Imaging 20:1131–1139.

Ashburner J, Friston KJ (1999): Nonlinear spatial normalization using basis functions. Hum Brain Mapp 7:254–266.

Back SA, Luo NL, Borenstein NS, Levine JM, Volpe JJ, Kinney HC (2001): Late oligodendrocyte progenitors coincide with the developmental window of vulnerability for human perinatal white matter injury. J Neurosci 21:1302–1312.

Basser PJ, Jones DK (2002): Diffusion-tensor MRI: Theory, experimental design and data analysis—A technical review. NMR Biomed 15:456–467.

Brett M, Johnsrude IS, Owen AM (2002): The problem of functional localization in the human brain. Nat Rev Neurosci 3:243–249.

Buecking A, Pfister R (2000): Sensory ataxia as the initial clinical symptom in X-linked recessive bulbospinal neuronopathy. J Neurol Neurosurg Psychiatry 69:277.

Butman JA, Floeter MK (2007): Decreased thickness of primary motor cortex in primary lateral sclerosis. AJNR Am J Neuroradiol 28:87–91.

Cedarbaum JM, Stambler N, Malta E, Fuller C, Hilt D, Thurmond B, Nakanishi A (1999): The ALSFRS-R: A revised ALS functional rating scale that incorporates assessments of respiratory function. BDNF ALS Study Group (Phase III). J Neurol Sci 169:13–21.

Chan S, Kaufmann P, Shungu DC, Mitsumoto H (2003): Amyotrophic lateral sclerosis and primary lateral sclerosis: Evidence-based diagnostic evaluation of the upper motor neuron. Neuroimaging Clin N Am 13:307–326.

Ciccarelli O, Catani M, Johansen-Berg H, Clark C, Thompson A (2008): Diffusion-based tractography in neurological disorders: Concepts, applications, and future developments. Lancet Neurol 7:715–727.

Ciccarelli O, Behrens TE, Johansen-Berg H, Talbot K, Orrell RW, Howard RS, Nunes RG, Miller DH, Matthews PM, Thompson AJ, Smith SM (2009): Investigation of white matter pathology in ALS and PLS using tract-based spatial statistics. Hum Brain Mapp 30:615–624.

Clement AM, Nguyen MD, Roberts EA, Garcia ML, Boillè S, Rule M, McMahon AP, Doucette W, Siwek D, Ferrante RJ, Brown RH Jr, Julien JP, Goldstein LS, Cleveland DW (2003): Wildtype non-neuronal cells extend survival of SOD1 mutant motor neurons in ALS mice. Science 302:113–117.

Dreha-Kulaczewski S, Dechent P, Helms G, Frahm J, Gartner J, Brockmann K (2006): Cerebral metabolic and structural alterations in hereditary spastic paraplegia with thin corpus callosum assessed by MRS and DTI. Neuroradiology 48:893–898.

Fink JK (2006): Hereditary spastic paraplegia. Curr Neurol Neurosci Rep 6:65–76.

Fink JK, Heiman-Patterson T, Bird T, Cambi F, Dube MP, Figlewicz DA, Haines JL, Hentati A, Pericak-Vance MA, Raskind W, Rouleau GA, Siddique T (1996): Hereditary spastic paraplegia: Advances in genetic research. Hereditary Spastic Paraplegia Working Group. Neurology 46:1507–1514.

Genovese CR, Lazar NA, Nichols T (2002): Thresholding of statistical maps in functional neuroimaging using the false discovery rate. Neuroimage 15:870–878.

Good CD, Scahill RI, Fox NC, Ashburner J, Friston KJ, Chan D, Crum WR, Rossor MN, Frackowiak RS (2002): Automatic differentiation of anatomical patterns in the human brain: Validation with studies of degenerative dementias. Neuroimage 17:29–46.

Guidetti D, Vescovini E, Motti L, Ghidoni E, Gemignani F, Marbini A, Patrosso MC, Ferlini A, Solime F (1996): X-linked bulbar and spinal muscular atrophy, or Kennedy disease: Clinical, neurophysiological, neuropathological, neuropsychological and molecular study of a large family. J Neurol Sci 135:140–148.

Harding AE (1993): Hereditary spastic paraplegias. Semin Neurol 13:333–336.

Jones DK, Symms MR, Cercignani M, Howard RJ (2005): The effect of filter size on VBM analyses of DT-MRI data. Neuroimage 26:546–554.

Karitzky J, Block W, Mellies JK, Traber F, Sperfeld A, Schild HH, Haller P, Ludolph AC (1999): Proton magnetic resonance spectroscopy in Kennedy syndrome. Arch Neurol 56:1465–1471.

Karlsborg M, Rosenbaum S, Wiegell M, Simonsen H, Larsson H, Werdelin L, Gredal O (2004): Corticospinal tract degeneration and possible pathogenesis in ALS evaluated by MR diffusion tensor imaging. Amyotroph Lateral Scler Other Motor Neuron Disord 5:136–140.

Kassubek J, Sperfeld AD, Baumgartner A, Huppertz HJ, Riecker A, Juengling FD (2006): Brain atrophy in pure and complicated hereditary spastic paraparesis: A quantitative 3D MRI study. Eur J Neurol 13:880–886.

Kassubek J, Juengling FD, Baumgartner A, Unrath A, Ludolph AC, Sperfeld AD (2007a)Different regional brain volume loss in pure and complicated hereditary spastic paraparesis: A voxel-based morphometric study. Amyotroph Lateral Scler 8:328–336.

Kassubek J, Juengling FD, Sperfeld AD (2007b)Widespread white matter changes in Kennedy disease: A voxel based morphometry study. J Neurol Neurosurg Psychiatry 78:1209–1212.

Kunimatsu A, Aoki S, Masutani Y, Abe O, Hayashi N, Mori H, Masumoto T, Ohtomo K (2004): The optimal trackability

threshold of fractional anisotropy for diffusion tensor tractography of the corticospinal tract. Magn Reson Med Sci 3:11–17.

La Spada AR, Roling DB, Harding AE, Warner CL, Spiegel R, Hausmanowa-Petrusewicz I, Yee WC, Fischbeck KH (1992): Meiotic stability and genotype-phenotype correlation of the trinucleotide repeat in X-linked spinal and bulbar muscular atrophy. Nat Genet 2:301–304.

Le Bihan D, Mangin JF, Poupon C, Clark CA, Pappata S, Molko N, Chabriat H (2001): Diffusion tensor imaging: concepts and applications. J Magn Reson Imaging 13:534–546.

Mader I, Karitzky J, Klose U, Seeger U, Sperfeld A, Naegele T, Schick F, Ludolph A, Grodd W (2002): Proton MRS in Kennedy disease: Absolute metabolite and macromolecular concentrations. J Magn Reson Imaging 16:160–167.

Mai JK, Assheuer J, Paxinos G (1997): Atlas of the Human Brain. San Diego: Academic Press. p 35.

McDermott C, White K, Bushby K, Shaw P (2000): Hereditary spastic paraparesis: A review of new developments. J Neurol Neurosurg Psychiatry 69:150–160.

Mueller HP, Unrath A, Ludolph AC, Kassubek J (2007a): Preservation of diffusion tensor properties during spatial normalization by use of tensor imaging and fibre tracking on a normal brain database. Phys Med Biol 52:N99–N109.

Mueller HP, Unrath A, Sperfeld AD, Ludolph AC, Riecker A, Kassubek J (2007b): Diffusion tensor imaging and tractwise fractional anisotropy statistics: Quantitative analysis in white matter pathology. Biomed Eng Online 6:42.

Mueller HP, Unrath A, Riecker A, Pinkhardt EH, Ludolph AC, Kassubek J (2009): Intersubject variability in the analysis of diffusion tensor images at the group level: Fractional anisotropy mapping and fiber tracking techniques. Magn Reson Imaging 27:324–334.

Mukherjee P, McKinstry RC (2006): Diffusion tensor imaging and tractography of human brain development. Neuroimaging Clin N Am 16:19–43.

Mukherjee P, Miller JH, Shimony JS, Philip JV, Nehra D, Snyder AZ, Conturo TE, Neil JJ, McKinstry RC (2002): Diffusion-tensor MR imaging of gray and white matter development during normal human brain maturation. AJNR Am J Neuroradiol 23:1445–1456.

Press WH, Flannery BP, Teukolsky SA, Vetterling WT (1992): Numerical Recipes in C: The Art of Scientific Computing. New York: Cambridge University Press. pp 636–639.

Pringle CE, Hudson AJ, Munoz DG, Kiernan JA, Brown WF, Ebers GC (1992): Primary lateral sclerosis. Clinical features, neuropathology and diagnostic criteria. Brain 115:495–520.

Rosenfeld A, Kak AC (1982): Digital Picture Processing, 2nd ed. Orlando: Academic Press. 349 p.

Sach M, Winkler G, Glauche V, Liepert J, Heimbach B, Koch MA, Buchel C, Weiller C (2004): Diffusion tensor MRI of early upper motor neuron involvement in amyotrophic lateral sclerosis. Brain 127:340–350.

Sage CA, Peeters RR, Gorner A, Robberecht W, Sunaert S (2007): Quantitative diffusion tensor imaging in amyotrophic lateral sclerosis. Neuroimage 34:486–499.

Salat DH, Tuch DS, Greve DN, van der Kouwe AJ, Hevelone ND, Zaleta AK, Rosen BR, Fischl B, Corkin S, Rosas HD, Dale AM (2005): Age-related alterations in white matter microstructure measured by diffusion tensor imaging. Neurobiol Aging 26:1215–1227.

Schreiber H, Gaigalat T, Wiedemuth-Catrinescu U, Graf M, Uttner I, Muche R, Ludolph AC (2005): Cognitive function in spinal- and bulbar-onset ALS. A longitudinal study in 52 patients. J Neurol 252:772–781.

Shen Y, Larkman DJ, Counsell S, Pu IM, Edwards D, Hajnal JV (2004): Correction of high-order eddy current induced geometric distortion in diffusion-weighted echo-planar images. Magn Reson Med 52:1184–1189.

Shibasaki Y, Tanaka H, Iwabuchi K, Kawasaki S, Kondo H, Uekawa K, Ueda M, Kamiya T, Katayama Y, Nakamura A, Takashima H, Nakagawa M, Masuda M, Utsumi H, Nakamuro T, Tada K, Kurohara K, Inoue K, Koike F, Sakai T, Tsuji S, Kobayashi H (2000): Linkage of autosomal recessive hereditary spastic paraplegia with mental impairment and thin corpus callosum to chromosome 15A13–15. Ann Neurol 48: 108–112.

Singer MA, Statland JM, Wolfe GI, Barohn RJ (2007): Primary lateral sclerosis. Muscle Nerve 35:291–302.

Smith SM, Jenkinson M, Johansen-Berg H, Rueckert D, Nichols TE, Mackay CE, Watkins KE, Ciccarelli O, Cader MZ, Matthews PM, Behrens TE (2006): Tract-based spatial statistics: Voxelwise analysis of multi-subject diffusion data. Neuroimage 31:1487–1505.

Snook L, Paulson LA, Roy D, Phillips L, Beaulieu C (2005): Diffusion tensor imaging of neurodevelopment in children and young adults. Neuroimage 26:1164–1173.

Soukup GR, Sperfeld AD, Uttner I, Karitzky J, Ludolph AC, Kassubek J, Schreiber H (2009): Frontotemporal cognitive function in X-linked spinal and bulbar muscular atrophy (SBMA): A controlled neuropsychological study of 20 patients. J Neurol 256:1867–1875.

Sperfeld AD, Karitzky J, Brummer D, Schreiber H, Haussler J, Ludolph AC, Hanemann CO (2002): X-linked bulbospinal neuronopathy: Kennedy disease. Arch Neurol 59:1921–1926.

Sperfeld AD, Kassubek J, Crosby AH, Winner B, Ludolph AC, Uttner I, Hanemann CO (2004): Complicated hereditary spastic paraplegia with thin corpus callosum: Variation of phenotypic expression over time. J Neurol 251:1285–1287.

Turner MR, Hammers A, Al-Chalabi A, Shaw CE, Andersen PM, Brooks DJ, Leigh PN (2007): Cortical involvement in four cases of primary lateral sclerosis using [^{11}C]-flumazenil PET. J Neurol 254:1033–1036.

Ulug AM, Grunewald T, Lin MT, Kamal AK, Filippi CG, Zimmerman RD, Beal MF (2004): Diffusion tensor imaging in the diagnosis of primary lateral sclerosis. J Magn Reson Imaging 19:34–39.

Vernooij MW, de Groot M, van der Lugt A, Ikram MA, Krestin GP, Hofman A, Niessen WJ, Breteler MM (2008): White matter atrophy and lesion formation explain the loss of structural integrity of white matter in aging. Neuroimage 43:470–477.